International Journal of Marine Science and Technology, vol. 2, no. 1, pp. 43–48, 2026 e-ISSN: 3093-3609
https://doi.org/10.65154/ijmst.35 https://i-jmst.vimaru.edu.vn

Optimal Design of an Acoustic Lens with Anisotropic Metamaterial

Van Nam Hoang* **and Minh Ngoc Nguyen**

Abstract: This paper employs advanced optimal techniques to design an acoustic lens composed of an anisotropic metamaterial. The structure of the optimized lens consists of random rigid scatters embedded in a matrix, in which the sizes of the scatters are treated as design variables of the optimization problem. The numerical examples demonstrate that the optimized lens can focus plane waves onto a focal region of subwavelength scale. At the focal distance of 1λ, the optimized design achieves subwavelength focusing, characterized by a full width at half maximum (FWHM) of 0.36λ, along with a high sound pressure level (SPL) of 14.7 dB at the focal point. This performance surpasses the diffraction limit, owing to the enhancement of evanescent waves through multiple scattering. Moreover, the optimized lens can offer a potential for a wide operating frequency range.

Keywords: Acoustic lens, anisotropic metamaterial, metamaterial, subwavelength focusing, superlens.

1. INTRODUCTION

Electromagnetic as well as acoustic waves emitted from a source (or object) consist of two components: propagating waves can propagate to the far-field, and evanescent waves decay exponentially in all natural materials. The evanescent waves that carry detailed information about the object cannot propagate far from the source. That is why the solution of a conventional lens is always limited by the diffraction limit [1] – the smallest distance between two points that can be resolved by a conventional lens system. In order to obtain a sub-wavelength solution, the evanescent waves need to be enhanced when they travel through the lens material. Metamaterial is a promising method to break the diffraction limit and gain sub-wavelength resolution. Until now, the metamaterials have been applied widely in imaging applications in both electromagnetic and acoustic wave fields [2,3,4].

Acoustic lensing applications, which play an important role in engineering and technology nowadays, are applied widely in many fields, for example: non-destructive testing, sea mapping, medical sonography, medical therapy, and so on. So, the efforts to break the diffraction limit and obtain sub-wavelength resolution are always of interest to researchers in the acoustic field. Many previous studies show that superlens based on acoustic metamaterial and phononic crystals have the possibility to manipulate and amplify the evanescent waves [4,5,6]. Superlens can give subwavelength imaging and focusing, but is typically limited to the near-field. The deep sub-wavelength imaging could be realized by using a planar superlens [7], a superlens using membrane-based metamaterials [8], and a metalens [9,10]. However, a major restriction of these lenses is that the object has to be placed very close to the lens to capture the evanescent waves. Otherwise, it is impossible to obtain subwavelength imaging on the focal plane.

When the distance between the object and the lens is sufficiently large, the waves emitted by the source can be approximated as plane waves when they reach the lens. Under plane-wave illumination, a conventional lens cannot produce a focal spot smaller than the diffraction limit, and therefore, sub-wavelength focusing becomes impossible. This physical limitation constrains the achievable resolution of many imaging and focusing systems used in practical fields such as medical diagnostics, ultrasound therapy, and underwater imaging. Some efforts to achieve acoustic sub-wavelength focusing with incident plane waves have been made: gradient index lens [11,12], three-dimensional acoustic lenses with axial symmetry [13], aperiodic flat lens [14]. Impressive results of acoustic focusing at the sub-wavelength scale were achieved with Fresnel lenses with an FWHM of 0.57λ at the focal distance of λ [15] and with multiple Fabry-Perot resonance effects with an FWHM of 0.21λ at the focal distance of $\lambda/70$ [16]. However, the lens in [16] performs well only when the

Manuscript received December 07, 2025; received in revised form January 15, 2026; accepted February 02, 2026; available online March 30, 2026.

Van Nam Hoang is with the School of Mechanical Engineering, Vietnam Maritime University, Haiphong, Vietnam (e-mail: namhv.vck@vimaru.edu.vn). Minh Ngoc Nguyen is with the Institute of Advanced Machines and Design, Seoul National University, Gwanak-ro 1, Seoul 08826, Republic of Korea (e-mail: nguyenminhngocsnu@snu.ac.kr).
* Corresponding author.

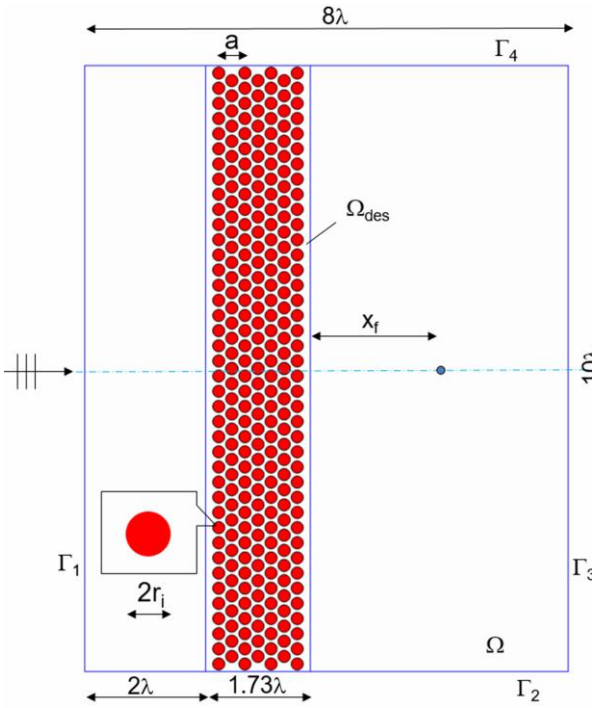

Fig.1. Schematic of an acoustic anisotropic metamaterial lens.

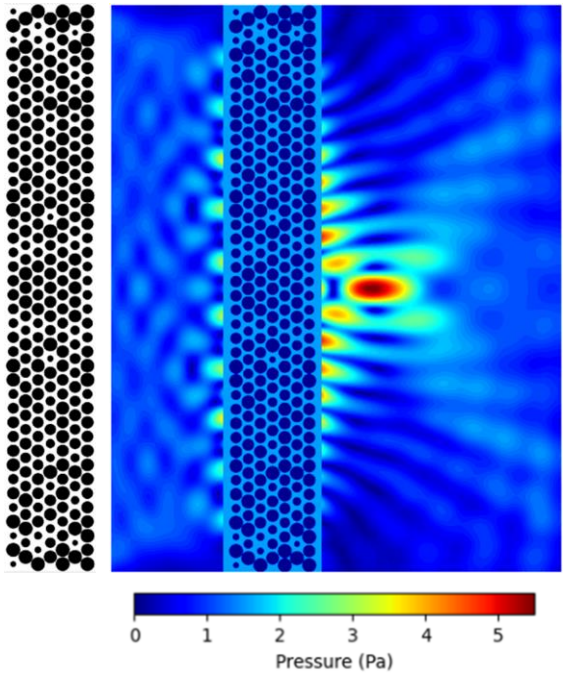

(a) (b)

Fig.2. Optimized results: (a) optimized design, (b) pressure field.

focal distance is positioned very close to the lens. Acoustic metamaterials and phononic crystals are typically fabricated with a periodic structure (unit cell), based on local resonance at a specific frequency, and are normally quite sensitive to frequency. This kind of material can be treated as a homogeneous medium when the unit-cell dimension is much smaller than the operating wavelength [17]. Anisotropic metamaterial is also used to obtain subwavelength focusing for acoustic waves [18,19]. The advantages of anisotropic metamaterial-based lenses lie not only in their ability to achieve subwavelength focusing under plane-wave illumination, but also in their capability to operate over a broad frequency range [20].

In this paper, we apply advanced optimal techniques to design an anisotropic metamaterial-based lens. Not restricted to focusing plane waves, the proposed method can also focus acoustic waves emitted from a point source into a subwavelength-scale focal region while achieving a high SPL.

Advanced optimization techniques have been widely used in structural engineering to obtain high-performance designs. Among these approaches, topology optimization based on element density [21] and the level set method [22] are particularly popular. In addition, alternative optimization frameworks have been proposed in [23–25], where the optimized topology is represented using the geometries of individual structural components. These optimization strategies have also been successfully applied to acoustic applications [26-28].

Motivated by these developments, this paper applies advanced optimization techniques to design an anisotropic metamaterial-based acoustic lens. Not restricted to focusing plane waves, the proposed method can also focus acoustic waves emitted from a point source into a subwavelength-scale focal region while achieving a high SPL. The lens consists of rigid scatters (cylinders) embedded in a matrix. The radii of the cylinders are treated as design variables that can be changed during the optimization process to modify the volume fraction and manipulate waves. The wave equation is solved with the finite element method. The method of moving asymptotes [29] is used for updating new variables in each iteration of the optimization procedure.

2. FORMULATION

2.1. Governing equation of acoustic waves

Suppose the problem is in the steady state. In a two-dimensional (2D) acoustic system, the wave propagation in an anisotropic medium in the frequency domain is described by the Helmholtz equation (1).

$$\nabla.(\rho^{-1}\nabla p) + \omega^2 \kappa^{-1} p = 0 \qquad (1)$$

where, p is the complex pressure field, ω is the angular frequency of the incident wave, ρ and κ are the mass density and bulk modulus of the local medium, respectively. $(\rho,\kappa) = (\rho_1,\kappa_1)$ for background medium (air) and $(\rho,\kappa) = (\rho_2,\kappa_2)$ for solid (epoxy). It is convenient to use relative material properties (ρ_r,κ_r).

$$\rho_r = \frac{\rho}{\rho_1} = \begin{cases} 1 & \text{(air)} \\ \dfrac{\rho_2}{\rho_1} & \text{(solid)} \end{cases} \qquad (2)$$

and

$$\kappa_r = \frac{\kappa}{\kappa_1} = \begin{cases} 1 & \text{(air)} \\ \dfrac{\kappa_2}{\kappa_1} & \text{(solid)} \end{cases} \tag{3}$$

Equation (1) can be rewritten as

$$\nabla.(\rho_r^{-1}\nabla p) + k_0^{\,2}\kappa_r^{-1} p = 0 \tag{4}$$

where, $k_0 = \omega / c_0$ is the wave number for air, c_0 is the sound speed in air.

In the model Fig.1, λ denotes the wavelength, and x_f denotes the focal distance. The incident plane waves enter on the left side of the computational domain Ω, the radiation condition is applied to the boundary Γ_1, a first-order absorbing boundary condition is applied to the boundaries $\Gamma_2, \Gamma_3, \Gamma_4$.

$$\begin{aligned} &\mathbf{n}.\nabla p + ik_0 p = 2ik_0 p_0 \quad (\text{on } \Gamma_1) \\ &\mathbf{n}.\nabla p + ik_0 p = 0 \qquad (\text{on } \Gamma_2, \Gamma_3, \Gamma_4) \end{aligned} \tag{5}$$

where, $\mathbf{n}$ is the normal unit vector of the boundary, p_0 is the pressure amplitude of the incident wave, and $i = \sqrt{-1}$.

By multiplying both sides of equation (4) by the weight function w, taking integration in the whole computational domain, and then applying Green's theory, the governing equation in strong form is transferred into the weak form (6):

$$\begin{aligned} &\int_\Omega \nabla w.(\rho_r^{-1}\nabla p)\,\mathrm{d}\Omega - k_0^{\,2}\int_\Omega \kappa_r^{-1} wp\,\mathrm{d}\Omega \\ &+ ik_0 \int_\Gamma \rho_r^{-1} wp\,\mathrm{d}\Gamma = 2ik_0 p_0 \int_\Gamma \rho_r^{-1} w\,\mathrm{d}\Gamma \end{aligned} \tag{6}$$

or equivalently

$$\mathbf{Sp} = \mathbf{f} \tag{7}$$

where, $\mathbf{p}$ is the vector of nodal values of the pressure field, $\mathbf{S}$ is the system matrix, and $\mathbf{f}$ is the nodal load vector.

2.2. Interpolation form

The objective of the optimization problem is to determine the material distribution within the design domain that yields the optimal performance responses. It is a discrete optimization problem. The final design should have either air or solid material at each point in the design domain. In this approach, the gradient of the objective function should be known before updating new variables during the optimization procedure [29]. Thus, for convenience in calculating the gradient of the objective function, a continuous variable γ_e $(0 \le \gamma_e \le 1)$ is introduced to control the distribution of materials for each element in the design domain. The value 0 corresponds to solid material, and the value 1 corresponds to air. The inverse interpolation form of density and bulk modulus [30] is recommended for the optimization problem.

$$1/\rho = 1/\rho_2 + \gamma_e(1/\rho_1 - 1/\rho_2) \tag{8}$$

and

$$1/\kappa = 1/\kappa_2 + \gamma_e(1/\kappa_1 - 1/\kappa_2) \tag{9}$$

The interpolation form in (8-9) leads to the intermediate values in the optimized design. In order to have the discrete values of 0 and 1 in the final design, we use a continuous approximation of the Heavisine function. Equation (10) allows for the conversion of the intermediate values of density into the nearly discrete values of 0 and 1.

$$\begin{aligned} \gamma_e &= \prod_{i=1}^{n} \frac{1}{1+\exp[-\beta(d_{ei} - r_i)]} \\ d_{ei} &= \sqrt{(x_e - x_i)^2 + (y_e - y_i)^2} \end{aligned} \tag{10}$$

where, d_{ei} is the distance from the centroid of element e to the center of the cylinder i, r_i is the radius of the cylinder i, n is the number of cylinders; $\beta = 10^4$ is a large number to obtain nearly 0–1 element density, $(x_e, y_e), (x_i, y_i)$ denotes coordinates of the centroid of element e and the center of the cylinder i, respectively.

2.3. Optimization formulation

In this paper, we use solid cylinders embedded in air to focus acoustic incident plane waves onto the focal region. In the 2D model (Fig.1), the lens profile includes zero-height cylinders, forming an equilateral triangle array of cylinders with a lattice distance a. Due to a very large difference in impedance between air and solid material $(\rho_2 c_2 / \rho_1 c_1 = 7648)$, these cylinders act as rigid scatterers. Thus, it is possible to neglect the waves that penetrate the rigid scatterers. Each rigid scatter can be modeled as an acoustic medium having sufficiently large impedance. The incident waves after entering the lens will scatter several times before going out of the lens. This type of scattering is the so-called multiple scattering. Each cylinder acts as a source of scattering waves. By changing the radius of each cylinder, we can control scattering waves and focus them onto a focal region. The goal of the optimization is to find the value of the radius of each cylinder to maximize pressure (or intensity) at the focal point. The SPL is evaluated as $10\log_{10}(|p_F|^2 / |p_{F0}|^2)$, in which $|p_F|$ is the absolute pressure at the focal point with the presence of the lens, $|p_{F0}|$ is the absolute pressure at the focal point without the lens. For incident plane waves, $|p_{F0}| = p_0$ (pressure magnitude of the plane waves). The optimization formulation has the form (11). It is not necessary to employ a volume constraint in the following problem:

$$\begin{aligned} &\text{Find } \mathbf{r} = \{r_1, r_2, ..., r_n\}^T \\ &\text{to minimize } \Phi = -\frac{|p_F|^2}{|p_{F0}|^2} \\ &\text{subject to } \quad r_l \le r_i \le r_u \end{aligned} \tag{11}$$

where, $\mathbf{r}$ is the vector of design variables, n is the number of design variables, r_l, r_u are the lower bound and the upper bound of design variables, respectively.

2.4. Sensitivity analysis

Sensitivity is needed for updating new variables in the optimization procedure. In this paper, the Adjoint method is employed to calculate derivatives of the objective function with respect to element densities γ_e, and then the gradients of the objective function with respect to design variables are calculated by using the change rule. The derivatives of the objective function with respect to element densities are derived by

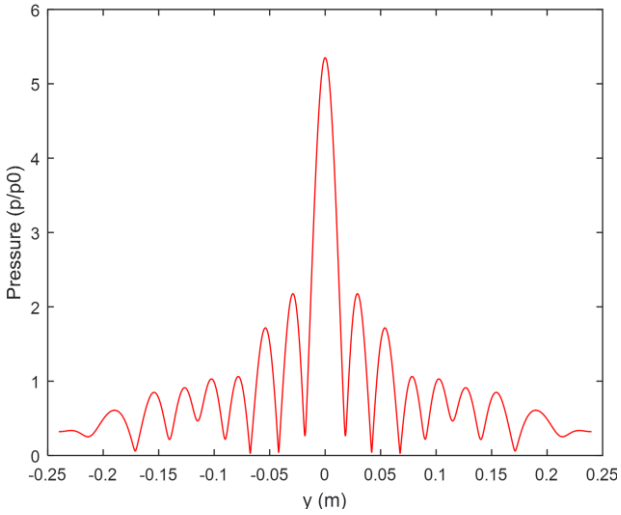

Fig.3. Pressure on the focal plane.

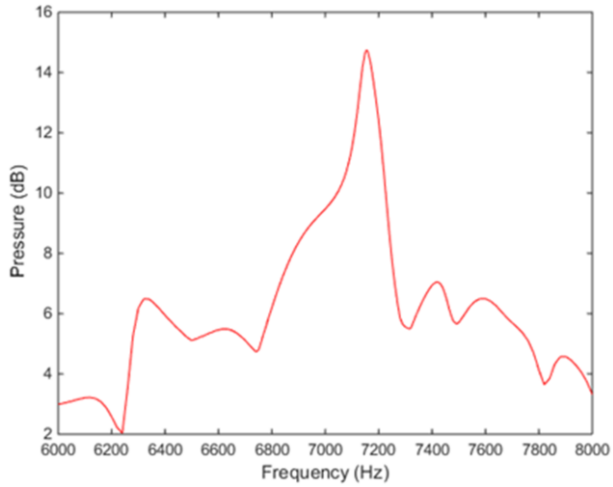

Fig.4. Frequency dependence of acoustic wave amplification.

$$\frac{\mathrm{d}\Phi}{\mathrm{d}\gamma_e}=\frac{\partial\Phi}{\partial\gamma_e}+\frac{\partial\Phi}{\partial\mathbf{p}}\frac{\partial\mathbf{p}}{\partial\gamma_e} \tag{12}$$

Equation (7) leads to

$$\frac{\partial\mathbf{S}}{\partial\gamma_e}\mathbf{p}+\mathbf{S}\frac{\partial\mathbf{p}}{\partial\gamma_e}=\frac{\partial\mathbf{f}}{\partial\gamma_e} \tag{13}$$

and

$$\frac{\partial\mathbf{p}}{\partial\gamma_e}=\mathbf{S}^{-1}\left(\frac{\partial\mathbf{f}}{\partial\gamma_e}-\frac{\partial\mathbf{S}}{\partial\gamma_e}\mathbf{p}\right) \tag{14}$$

Insert equation (14) into (12) yields

$$\frac{\mathrm{d}\Phi}{\mathrm{d}\gamma_e}=\frac{\partial\Phi}{\partial\gamma_e}+\frac{\partial\Phi}{\partial\mathbf{p}}\mathbf{S}^{-1}\left(\frac{\partial\mathbf{f}}{\partial\gamma_e}-\frac{\partial\mathbf{S}}{\partial\gamma_e}\mathbf{p}\right) \tag{15}$$

and

$$\frac{\mathrm{d}\Phi}{\mathrm{d}\gamma_e}=\frac{\partial\Phi}{\partial\gamma_e}+\boldsymbol{\lambda}^T\left(\frac{\partial\mathbf{f}}{\partial\gamma_e}-\frac{\partial\mathbf{S}}{\partial\gamma_e}\mathbf{p}\right) \tag{16}$$

where,

$$\boldsymbol{\lambda}=\left(\frac{\partial\Phi}{\partial\mathbf{p}}\mathbf{S}^{-1}\right)^T=\left(\mathbf{S}^T\right)^{-1}\left(\frac{\partial\Phi}{\partial\mathbf{p}}\right)^T \tag{17}$$

and

$$\mathbf{S}^T\boldsymbol{\lambda}=\left(\frac{\partial\Phi}{\partial\mathbf{p}}\right)^T=\{0,...,-\frac{\bar{p}_F}{|p_{F0}|^2},...,0\}^T \tag{18}$$

where $\bar{p}_F$ is the complex conjugate of p_F. It was proved in [27] that equation (16) is equivalent to equation (19)

$$\frac{\mathrm{d}\Phi}{\mathrm{d}\gamma_e}=\frac{\partial\Phi}{\partial\gamma_e}+2\mathrm{Re}\left[\boldsymbol{\lambda}^T\left(\frac{\partial\mathbf{f}}{\partial\gamma_e}-\frac{\partial\mathbf{S}}{\partial\gamma_e}\mathbf{p}\right)\right] \tag{19}$$

where, $\partial\Phi/\partial\gamma_e$=0, $\partial\mathbf{f}/\partial\gamma_e=0$ for this problem.

Applying the change rule, one gets

$$\frac{\mathrm{d}\Phi}{\mathrm{d}r_i}=\sum_{e=1}^{N}\frac{\mathrm{d}\Phi}{\mathrm{d}\gamma_e}\frac{\mathrm{d}\gamma_e}{\mathrm{d}r_i} \tag{20}$$

where, N is the number of elements in the design domain Ω_{des}. The sensitivities $\mathrm{d}\gamma_e/\mathrm{d}r_i$ can be derived from equation (10) as

$$\frac{\mathrm{d}\gamma_e}{\mathrm{d}r_i}=-\gamma_e\frac{\beta\exp[-\beta(d_{ei}-r_i)]}{1+\exp[-\beta(d_{ei}-r_i)]} \tag{21}$$

3. EXAMPLES

3.1. Focusing plane waves

In the numerical simulation, we set the frequency of the incident wave $f=7154.67$ Hz and the pressure magnitude $p_0=1$ Pa. Material properties: air ($\rho_1=1.204$ kg/m^3, $c_1=343.42\ m/s$), solid (epoxy) ($\rho_2=1180$ kg/m^3, $c_2=2680\ m/s$). The wavelength of the waves propagating in air $\lambda=48\ mm$, the lattice distance $a=\lambda/4$, the lower bound, the upper bound $r_l=1\ mm$, $r_u=a/2$, and the focal distance $x_f=\lambda$. In the initial design, Fig.1, all radii are chosen with the same value of $0.4a$. Fig.2a shows the optimized lens. The distribution of the pressures is shown in Fig.2b. The SPL is 14.7 dB obtained at the focal point on the focal plane. The wave focuses on the focal region with an FWHM of 0.36λ (see Fig. 3), which is smaller than the FWHM of $\approx 0.5\lambda$ in [15,32]. The optimized lens is capable of generating the focal spot beyond the diffraction limit (0.5λ). This implies that evanescent waves are enhanced when propagating through the optimized lens. The detailed information is transferred to the image after the lens.

Acoustic isotropic metamaterial-based lenses typically work based on the local resonant principle and thus can only work well with a narrow range of operating frequencies. This has been discussed in [7,16]. An acoustic anisotropic metamaterial-based lens, which is designed by manipulating the scattering waves, might be recognized with a wide operating frequency range. To investigate the frequency dependence of SPL of the designed lens, we vary the frequency of the incident waves from 6000 to 8000 Hz and measure SPL at the focus point (Fig.4). High SPL and subwavelength focusing are obtained with a wide range of frequencies. For example, the subwavelength focusing is recognized

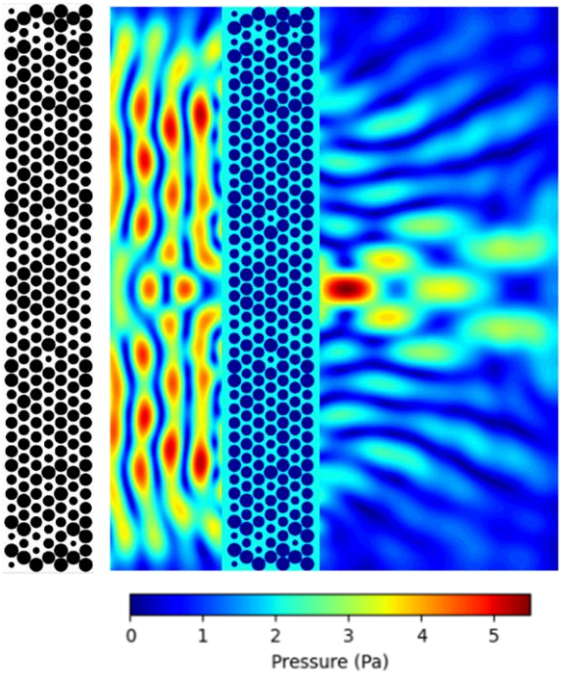

(a) (b)

Fig.5. The optimized lens works at a frequency of 6900 Hz.

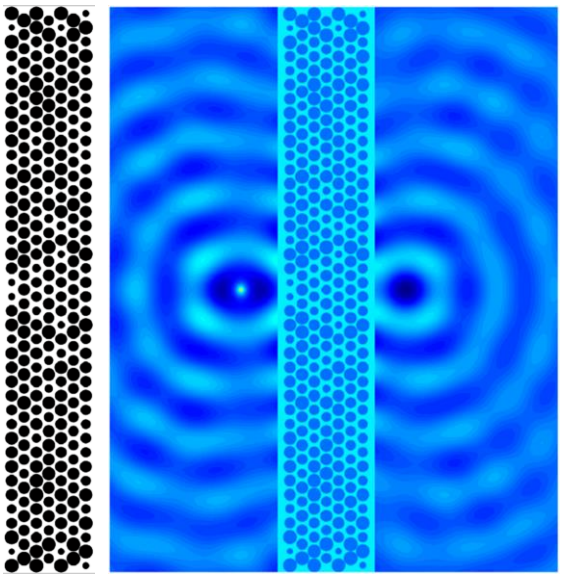

(a) (b)

Fig.6. (a) optimized design, (b) pressure pattern, light and dark regions denote positive and negative pressure fields.

for the range of frequency from 6275 Hz ($\text{FWHM} = 0.45\lambda$) to 7765 Hz ($\text{FWHM} = 0.44\lambda$) with SPL larger than 5 dB. The lens gives the best resolution at a frequency of 7154.67 Hz with an FWHM of 0.36λ and lower resolutions at the other frequencies. This represents a significant advantage of the acoustic anisotropic metamaterial lens. Fig.5 illustrates the lens performance at a frequency of 6900 Hz, where an FWHM of 0.39 λ and a SPL of 8.4 dB are achieved at the focal point, with only a slight shift in the focusing position.

Evanescent waves behind the lens decay exponentially, so their contribution to focusing depends on the position of the focal point. To maximize the effect of these evanescent components, the optimization should be performed with the focal plane located close to the lens. The numerical simulations show that subwavelength focusing is obtained with an FWHM of 0.85λ, 0.56λ, 0.36λ at $x_f = 8\lambda, 4\lambda, 1\lambda$, respectively. The near focusing was also investigated in this study. The optimization problem performed with the focal distance of 0.25λ gives subwavelength resolution with an FWHM of 0.25λ and with an extremely high SPL of 23 dB.

3.2. Focusing waves emitted from a point source

Not limited to focusing plane waves, this method can also be employed to design a superlens. In this scenario, a point source is positioned near the lens instead of using incident plane waves. All parameters from the model in Fig. 1 are retained, except that the incident plane wave is replaced by the point source and the positions of the point source (from the left side) $x_s = 0.75\lambda$, the position of the focal point $x_f = 0.5\lambda$, and the distance from the left side of the computational domain to the left side of the lens 3λ. Many previous studies [31] have highlighted the importance of a critical distance $x_s + x_f = d$ (d - the thickness of the lens) when designing isotropic metamaterial-based superlenses. In contrast, the proposed method does not require this constraint, and the lens distances x_s, x_f can be chosen arbitrarily. Under these conditions, the phase of the image does not need to match that of the source. This also represents a significant difference between isotropic and anisotropic metamaterial-based lenses. The Fig.6 shows the optimized result of designing a superlens. In which, subwavelength focusing is obtained with an FWHM of 0.28λ and with a very high SPL of 18 dB at the focal point.

4. CONCLUSION

Advanced optimization techniques were employed to design an acoustic anisotropic metamaterial lens. The lens is composed of rigid scatterers embedded in air, and the optimization process involves adjusting the sizes of these scatterers. The optimized lens is capable of focusing acoustic plane waves onto a subwavelength-scale focal region, achieving a very high sound pressure level at the focal point. Moreover, the optimized lens demonstrates potential for operation over a wide frequency range. The proposed method can also be applied to the design of a superlens for focusing waves emitted from a point source.

REFERENCES

[1] R. G. Maev, *Acoustic microscopy fundamentals and applications*, WILEY-VCH Verlag GmbH & Co., 2008.

[2] S. Zhang, L. Yin, and N. Fang, “Focusing ultrasound

with an acoustic metamaterial network," *Physical Review Letters*, vol. 102, 2009.
[3] X. Zhang and Z. Liu, "Negative refraction and focusing of ultrasound in two-dimensional phononic crystals," *Applied Physics Letters*, vol. 85, no. 341, 2004.
[4] Q. Lu et al., "Perspective: Acoustic metamaterials in future engineering," *Engineering*, vol. 17, 2022.
[5] X. Zhou, M. B. Assouar, and M. Oudich, "Acoustic superfocusing by solid phononic crystals," *Applied Physics Letters*, vol. 105, 2014.
[6] Y. Zhou et al., "Acoustic metamaterial lens for two-dimensional vortex beamforming and perception," *International Journal of Mechanical Sciences*, vol. 286, 2025.
[7] H. Jia et al., "Subwavelength imaging by a simple planar acoustic superlens," *Applied Physics Letters*, vol. 97, 2010.
[8] J. J. Park et al. "Acoustic superlens using membrane-based metamaterials," *Applied Physics Letters*, vol. 106, 2015.
[9] Y. Cheng et al., "Acoustic subwavelength imaging of subsurface objects with acoustic resonant metalens," *Applied Physics Letters*, vol. 103, 2013.
[10] J. Zhu et al., "A holey-structured metamaterial for acoustic deep-subwavelength imaging," *Nature Physics*, vol. 7, no. 52, 2011.
[11] S. Peng et al., "Acoustic far-field focusing effect for two-dimensional graded negative refractive-index sonic crystals," *Applied Physics Letters*, vol. 96, 2010.
[12] Z. Wang et al., "Focusing of liquid surface waves by gradient index lens," *Europhysics Letters*, vol. 108, 2014.
[13] L. Sanchis et al., "Three-dimensional acoustic lenses with axial symmetry, *Applied Physics Letters*, vol. 97, 2010.
[14] J. T. Welter et al., "Focusing of longitudinal ultrasonic waves in air with an aperiodic flat lens," *The Journal of the Acoustical Society of America*, vol. 130, 2011.
[15] M. Moleron, M. Serra-Garcia, and C. Daraio, "Acoustic Fresnel lenses with extraordinary transmission," *Applied Physics Letters*, vol. 105, 2014.
[16] Z. Lin et al., "Acoustic focusing of sub-wavelength scale achieved by multiple Fabry-Perot resonance effect," *Journal of Applied Physics*, vol. 115, 2014.
[17] D. Torrent and J. Sánchez-Dehesa, "Acoustic metamaterials for new two-dimensional sonic devices," *New Journal of Physics*, vol. 9, 2007.
[18] V. Romero-García et al., "Wave focusing using symmetry matching in axisymmetric acoustic gradient index lenses," *Applied Physics Letters*, vol. no. 103, 2013.
[19] F. Ma et al., "Acoustic focusing and imaging via phononic crystal and acoustic metamaterials," *Journal of Applied Physics*, vol. 131, 2022.
[20] G. D'Aguanno et al., "Broadband metamaterial for nonresonant matching of acoustic waves," *Scientific Reports*, vol. 2, 2012.
[21] M. P. Bendsoe and N. Kikuchi, "Generating optimal topologies in structural design using a homogenization method," *Computer Methods in Applied Mechanics and Engineering*, vol. 71, 1988.
[22] J. A. Sethian and A. Wiegmann, "Structural boundary design via level set and immersed interface methods," *Journal of Computational Physics*, vol. 163, 2000.
[23] V. N. Hoang, H. B. Nguyen, and X. H. Nguyen, "Explicit topology optimization of nearly incompressible materials using polytopal composite elements," *Advances in Engineering Software*, vol. 149, 2020.
[24] V. N. Hoang and X. H. Nguyen, "Extruded-geometric-component-based 3D topology optimization," *Computer Methods in Applied Mechanics and Engineering*, vol. 371, 2020.
[25] V. N. Hoang, X. Wang, and X. H. Nguyen, "A three-dimensional multiscale approach to optimal design of porous structures using adaptive geometric components," *Composite Structures*. vol. 273, 2021.
[26] G. H. Yoon et al., "Topology optimization for acoustic structure interaction problems," *International Journal for Numerical Methods in Engineering*, vol. 70, 2007.
[27] J. H. Kook et al., "Acoustical topology optimization for Zwicker's loudness model – Application to noise barriers," *Computer Methods in Applied Mechanics and Engineering*, vol. 237, 2012.
[28] K. H. Kim and G. H. Yoon, "Acoustic topology optimization using moving morphable components in neural network-based design," *Structural and Multidisciplinary Optimization*, vol. 65, 2022.
[29] K. Svanberg, "The method of moving asymptotes-a new method for structural optimization," *International Journal for Numerical Methods in Engineering*, vol. 24, 1987.
[30] M. B. Dühring, J. S. Jensen, and O. Sigmund, "Acoustic design by topology optimization," *Journal of Sound and Vibration*, vol. 317, 2008.
[31] J. B. Pendry, "Negative refraction makes a perfect lens," *Physical Review Letters*, vol. 85, 2000.
[32] S. C. Ibáñez et al., "Cylindrical 3D printed configurable ultrasonic lens for subwavelength focusing enhancement," *Scientific Reports*, vol. 10, 2020.